Case Studies in Engineering Failure Analysis 7 (2016) 17–23

Contents lists available at ScienceDirect

Case Studies in Engineering Failure Analysis

journal homepage: www.elsevier.com/locate/csefa

Short communication

Failure analysis of a half-shaft of a formula SAE racing car

A.V. Guimaraes [a,*], P.C. Brasileiro [b], G.C. Giovanni [b], L.R.O. Costa [b], L.S. Araujo [b]

[a] Universidade Federal Rural do Rio de Janeiro, Rio de Janeiro, Brazil
[b] Escola Politécnica, Universidade Federal do Rio de Janeiro, Rio de Janeiro, Brazil

ARTICLE INFO

Article history:
Received 27 November 2015
Received in revised form 30 April 2016
Accepted 3 May 2016
Available online 9 May 2016

Keywords:
Half-shaft
Overload fracture
Torsional fatigue

ABSTRACT

The formula SAE is a competition among students worldwide, where they are challenged to design, build and test a small formula-type racing car, following rules and specifications defined by the Society of Automotive Engineers (SAE). In the present analysis, a premature failure of a half-shaft of the transmission system of a racing car occurred after circa 100 km of use. The fractured component was analyzed by means of metallographic, chemical and mechanical analysis, fractography and finite element analysis. The results show that the alloy steel bar used for the half-shaft did not follow specifications, with a consequent lower strength and resulting in a material with insufficient loading capacity and fatigue resistance. As a consequence, the fracture process was a confluence of torsional fatigue crack propagation and overload ductile fracture through the spline section of the half-shaft.

1. Background

The formula SAE is a competition among students worldwide, where they are challenged to design, build and test a small formula-type racing car following rules and specifications defined by the Society of Automotive Engineers (SAE). The prototype is a tubular-structure, rear wheel drive car, powered by a 600 cc motorbike engine. The power produced by the engine is transmitted to the wheel via a half-shaft, which is connected to the differential coupling at the inner end and to the wheel at the outer end. Constant-velocity (CV) joints are used on both ends of the half-shaft, in order to provide a certain degree of angular displacement. The torque is transmitted to and from the half-shaft via splines on both ends of the component. Therefore, transmission shafts are subjected to significant stresses caused by bending and torsional moments [1,2]. Fig. 1 shows the half-shaft assembled to the differential and the wheel and the detail of the outer end and the CV joint connected to the wheel.

As spline shafts are usually submitted to fluctuating or vibratory loads, fatigue is a primary cause of failure, especially on stress raisers like the spline roots [3,4]. Impacts or transitional loads can also lead to overload failures [2,4–6].

In the present study, a failure of a half-shaft was analyzed by means of microstructural and mechanical characterization and fractography. The stress distribution along the half-shaft was determined by finite element (FE) analysis. The half-shaft fractured during the test of the car on the racing track – after only circa of 100 km of test distance – when the expected racing

* Corresponding author at: Centro de Tecnologia da UFRJ, Bl. F, F-214 – Ilha do Fundão, Rio de Janeiro, CEP 21941-972, Brazil.
E-mail address: aleengmat@poli.ufrj.br (A.V. Guimaraes).

http://dx.doi.org/10.1016/j.csefa.2016.05.002

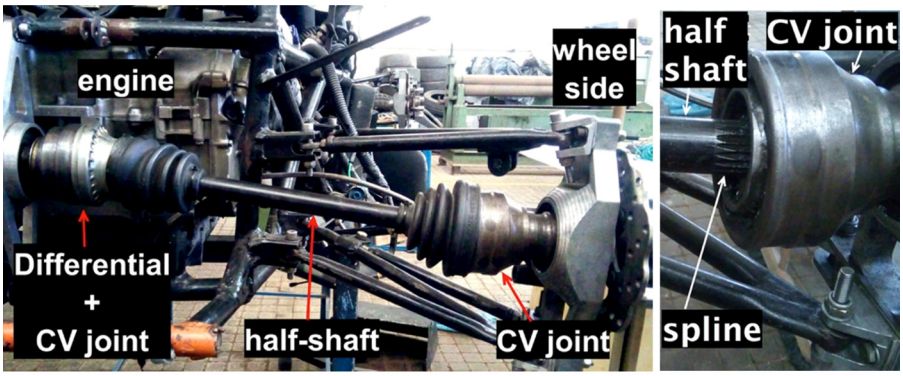

Fig. 1. Connection between the half-shaft and the CV joint connected to the wheel. On the end of the shaft a machined spline is present.

life of the component is 500 km. The fracture occurred when the car completed a curve and initiated the straight part of the track. In this situation, an increasing torque is induced, in order to increase the velocity of the car.

2. Investigation methods

The failed half-shaft was collected for visual analysis. The fracture surface on one of the fractured parts of the component was protected to avoid damage to the fracture surface [7] and cut at 10 mm from the spline. The other part of the half-shaft was stuck inside the CV joint and the fracture surface was damaged during the removal from the joint. Even damaged, this part of the component was taken for analysis. As a cleaning procedure, the fracture surface was immersed in alcohol under ultrasonic agitation. The fractography was obtained via scanning electron microscopy (SEM) with secondary electrons and acceleration voltage of 20 kV. Shortly before the SEM analysis, the sample was immersed in Clarke's solution to remove oxidation from the fracture surface.

Samples for microstructural and mechanical characterization and chemical analysis were cut from the remaining section of the half-shaft. The metallographic preparation consisted of grinding with emery paper up to 1200 mesh and polishing with diamond paste up to 1 μm. The microstructure was revealed with Nital reagent and analyzed by SEM on secondary electrons mode. For the mechanical characterization, Rockwell C hardness measurements and tensile tests were performed on the samples. The chemical analysis was obtained via optical emission spectroscopy.

The finite element (FE) method was applied to analyze the stress distribution in the surroundings of the fractured region of the half-shaft. The geometry of the half-shaft, CV joint and assembly were produced using the FreeCad® open source software and the FE analysis was conducted with the Deform-3D® package. The mesh was generated using the Gmsh open source FE mesh generator, using a tetrahedral element with linear approximation. The mesh at the spline region, where the failure occurred, was refined. Contact and friction stresses were taken into account, as well as the friction coefficient considered lubrication of the contact between the half-shaft and the CV joint. Fig. 2 shows the assembly and the detail of the connection of the half-shaft with the CV joint on the wheel side.

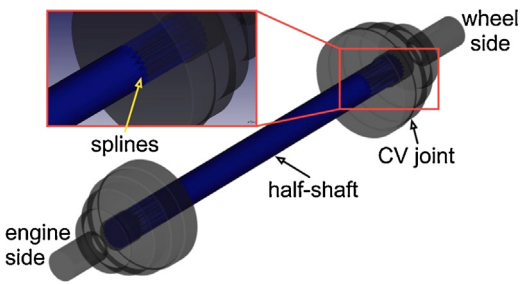

Fig. 2. Assembly of the half-shaft and the CV joints. In detail, the connection of the half-shaft with the CV joint on the wheel side.

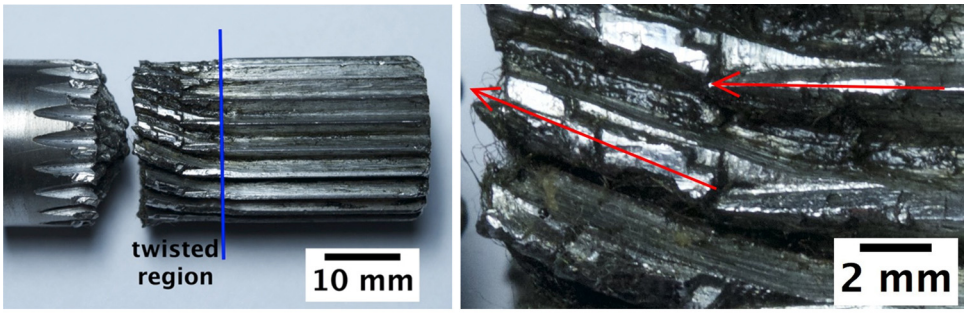

Fig. 3. (a) The fracture on the spline section of the half-shaft. The fracture was normal to the longitudinal axis of the component. A detailed view of the twisted region is shown in (b) with the red arrows indicating the alignment of the top part of the spline thread.

3. Results and discussion

3.1. Visual analysis

Fig. 3a shows the lateral view of both fractured parts. The fracture surface was mainly normal to the longitudinal axis of the shaft, the central part presenting a cup-and-cone morphology. Observation of the splines of the half-shaft part removed from the CV joint revealed plastic deformation, resulting in contortion of the splines. This morphology and a fracture surface normal to the half-shaft longitudinal axis was observed in [2,5,6] and associated to a torsional overload ductile fracture. Additionally, at the contorted region, two different morphologies were observed. Adjacent to the fracture surface, the splines were fully twisted from the top to the bottom of the thread. While at circa 5 mm from the fracture the top part of the spline was parallel to the longitudinal axis, whilst the lower part followed the twist of the previous distorted region. This morphology is presented in detail in Fig. 3b. The twisting angle was approximately 20°. The double twisted morphology could be associated to the fact that the half-shaft has a relative freedom of axial movement inside the CV joint [8].

Fig. 4 shows the transverse view of the fracture surface. An irregular and opaque morphology was observed. A similar morphology was observed by Brown [9] and associated with torsional fatigue fracture.

4. Fractography

Detailed observation of the fracture surface presented in Fig. 4 was obtained by SEM analysis, as shown in Fig. 5. The images were taken at specific points: close to the edge; at a quarter-radius from the edge; mid-radius and; at center of the fracture surface. Part of the surface was damaged due to rubbing. However, a significant part of the fracture was preserved and dimple morphology was evidenced. The elongated dimples close to the surface, as shown in Fig. 5a, were also observed

Fig. 4. Transverse view of the fracture surface.

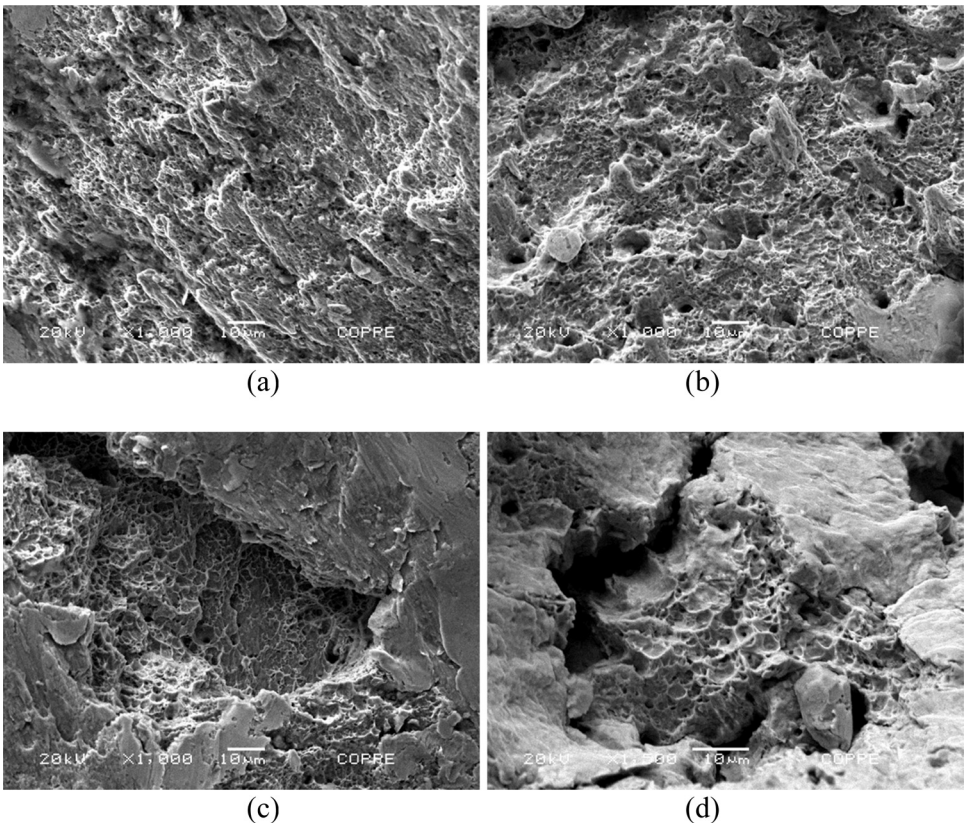

Fig. 5. Fracture morphology: (a) close to the edge; (b) at a quarter-radius from the edge; (c) at mid-radius; (d) at the center of the fracture surface.

by Varin [5] and associated with the larger shear deformations in that region. Additionally, besides the elongated dimples, secondary cracks were observed. Fig. 6 shows a lateral view of the spline close to the fracture surface, revealing several small transverse cracks and a large longitudinal crack emanating from the spline root. Transverse observation of the half-shaft close to the fracture confirmed that the large cracks emanated from several spline roots. Furthermore, other secondary cracks were observed, as presented in Fig. 7. In the same figure, it is possible to see that the tips of the spline treads were worn away from the component. Sinha et al. [3] also evidenced cracks emanating from the spline roots, and associated them to a fatigue process due to torsional loading. A similar morphology was observed by Thielen and Fine [10] as well, after fatigue tests on AISI/SAE 4140 steel samples.

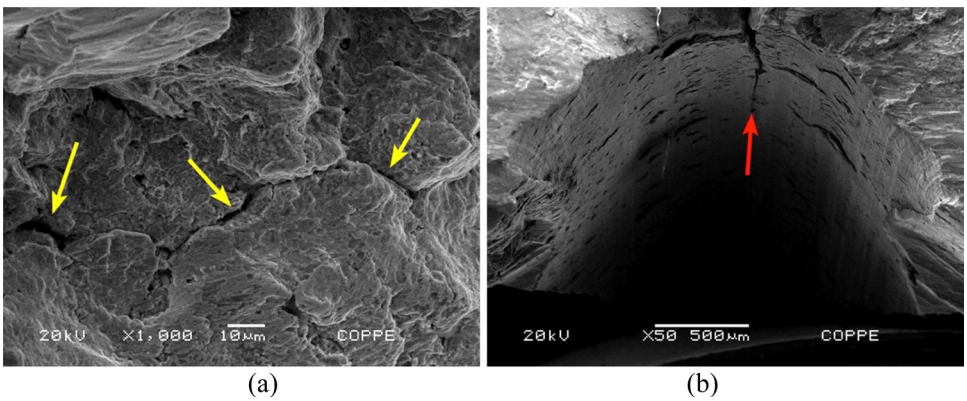

Fig. 6. (a) Secondary cracks observed on the fracture surface close to the edge (yellow arrows); (b) spline region with intense transverse cracking and a longitudinal crack at the base of the spline root (red arrow).

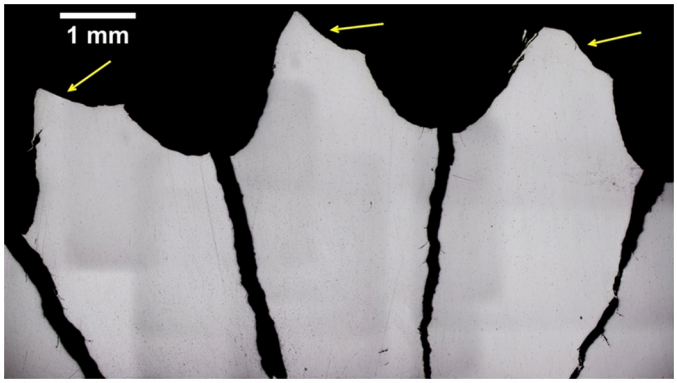

(a)

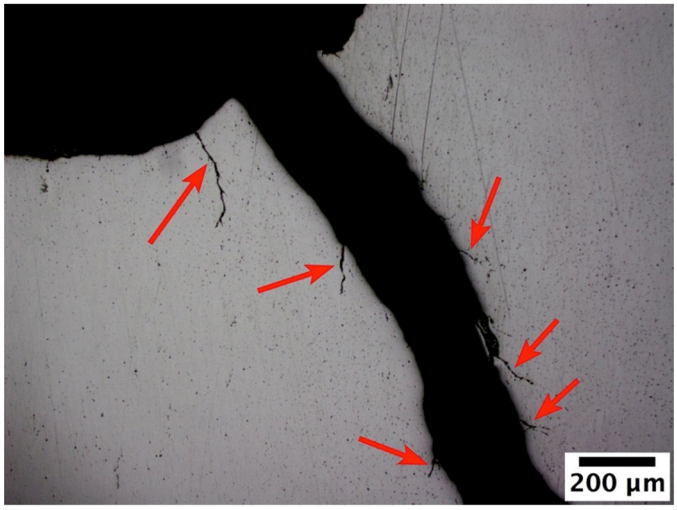

(b)

Fig. 7. Transverse view of the half-shaft close to the fracture surface: (a) large cracks emanate from the roots of the splines and the wear of the splines (yellow arrows); (b) secondary cracks (red arrows) observed inside the crack.

5. Chemical analysis and microstructural characterization

Chemical analysis of the half-shaft is presented in Table 1. Based on its composition, the alloy was classified as an AISI/SAE 4140 steel [11]. However, the project specifications and strength requirements for the component considered a 4340 steel in a quenched and tempered microstructural condition.

The SEM observation of the microstructure through the transverse section of the half-shaft revealed a bainitic microstructure [12,13]. No evidence of surface treatment of the spline threads was observed. Fig. 8 shows the micrographs of the half-shaft.

6. Mechanical properties

The mechanical properties were measured by means of hardness measurements (Rockwell C) and a tensile test. The hardness measurements points were located on the transverse section of the bar at regions close to the edge and in the

Table 1
Chemical composition of the material (wt.%).

	C	Si	Mn	P	S	Cr	Ni	Mo	Nb	Cu	Al	Fe
This work	0.410	0.238	0.810	0.038	0.022	0.950	0.051	0.128	0.020	0.011	0.018	Bal.
AISI/SAE 4140 [11]	0.38 0.43	0.15 0.35	0.75 1.00	0.035 max.	0.040 max.	0.80 1.10	–	0.15 0.25	–	–	–	Bal.

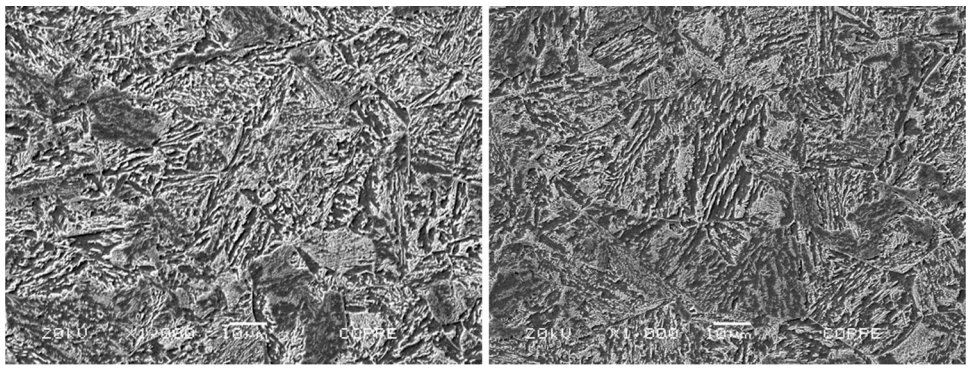

Fig. 8. Microstructure of the half-shaft: (a) close to the surface; (b) at the center. In both cases a bainitic microstructure was identified.

center, with three measurements for each region. Table 2 presents the Rockwell C hardness values. As no significant change of microstructure and hardness through transverse section was observed, in order to provide more precise information regarding properties for the finite element simulation, a tensile test was conducted on a specimen machined from the center region of the bar and based on ASTM E8 Standard [14]. It is important to remark that, due to the limitation of the available material for tensile specimens, only one sample was evaluated, with an engineering strain rate of $4 \times 10^{-4}\,s^{-1}$. Table 3 shows the mechanical properties determined by the tensile test and the comparison with the values for the specified AISI/SAE 4340 steel in a quenched and tempered condition (austenitized at 850 °C for 30 min, quenched in oil and tempered at 500 °C for 2 h).

Based on the microstructure observed and the mechanical properties measured, it was evidenced that the half-shaft used was on a normalized condition, while the specified condition required quenched and tempered microstructure, in order to achieve the desired properties. It is important to remark, as described in the previous section, that not only the microstructure was different from the necessary, as the alloy composition itself. The AISI/SAE 4340 steel presents higher strength and hardenability than the AISI/SAE 4140 steel.

7. Finite elements analysis

The finite element analysis was conducted in the region where the half-shaft is connected to the CV joint, as presented in Fig. 9. It was possible to observe that a high stress concentration was localized in the region of the spline filet, which is in agreement with the observed fracture region (Fig. 3(a)) and the work of Leen et al. [16]. Comparing the effective stress values calculated versus the strength of the AISI/SAE 4140 steel, at the region of the spline filet, the yield strength of the half-shaft (665 MPa) was surpassed by the effective stress, which is related to a torque of 590 N m (65% of the 950 N m design requirement). The maximum stress was observed at the face of the spline teeth, where the contact with the CV joint occurs [17,18]. The value achieved was higher than the yield strength (665 MPa). This result is corroborated by the observations of wear on the face of the spline teeth (Fig. 7(a)) and the localized plastic deformation (Fig. 3(a) and (b)).

Table 2
Rockwell C (HRC) hardness measurements on the transverse section of the half-shaft.

Position	HRC
Center	36.9 ± 0.1
Edge	37.7 ± 0.3

Table 3
Mechanical properties from tensile test.

Property	Specimen from the half-shaft	AISI/SAE 4340, quenched and tempered [15]
Yield strength	665 MPa	1110 MPa
Ultimate tensile strength	916 MPa	1294 MPa
Elongation	12.8%	14%
Reduction of area	52.6%	50%

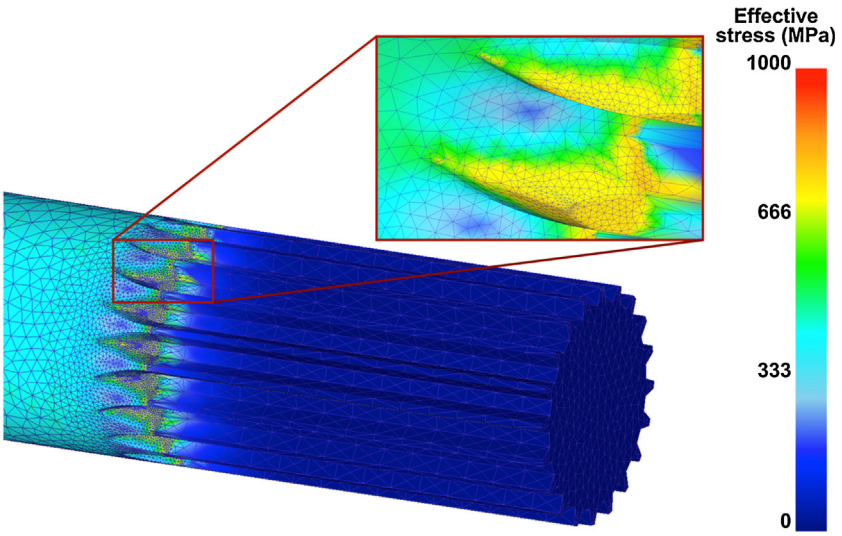

Fig. 9. Effective stress distribution on the surface of the half-shaft. Stresses higher than the yield strength of the alloy were observed at the filet region of the spline (in detail).

8. Conclusion

Based on the observations, the following conclusions can be made:

- The use of a AISI/SAE 4140 steel instead of the specified AISI/SAE 4340 steel had a decisive influence on the premature failure of the component, as the lower hardenability and strength resulted in a microstructure with insufficient mechanical properties for the requisites of the half-shaft.
- The failure of the half-shaft occurred by a combination of torsional fatigue and overload. Fatigue cracks were nucleated at the root of the spline, which reduced the loading capacity of the component. Plastic deformation due to overload occurred on multiple events, evidenced by the twisted threads and the fracture surface.
- The finite element analysis has shown that the higher stresses were observed at the filet at the spline region, especially at the face of the spline teeth, corroborated by the wear observed in these regions.

References

[1] Naunheimer H, Bertsche B, Novak W, Ryborz J. Automotive transmissions: fundamentals, selection, design and application. 2nd ed. Berlin: Springer-Verlag; 2011.
[2] Lin CY, Hung JP, Hsu TC. Failure analysis of reverse shaft in the transmission system of all-terrain vehicles. J Fail Anal Prev 2008;8:75–80.
[3] Sinha P, Bhattacharyya S. Failure investigation of spline-shaft of an under slung crane. J Fail Anal Prev 2013;13:601–6.
[4] Bonnett AH. Cause, analysis and prevention of motor shaft failures. In: IEEE Conf Rec Annu Pulp Pap Ind Tech Conf. 1998. p. 166–80.
[5] Varin JD. Fracture characteristics of steering gear sector shafts. Pract Fail Anal 2002;2:65–9.
[6] Li YJ, Zhang WF, Tao CH. Fracture analysis of a castellated shaft. Eng Fail Anal 2007;14:573–8.
[7] Van der Voort GF. Microscopic examination procedures for failure analysis. In: McCall , French , editors. Symp. Metallogr. Fail. Anal.. Houston: Plenum Press; 1977. p. 33–63.
[8] Churches A. Shafts and bearings. Gen. Notes Eng. Hardw.. School of Mechanical and Manufacturing Engineering, The University of New South Wales; 2010.
[9] Brown T. Torsional fatigue failures: identification diagnosis and prevention. Uptime Mag 2014;20–2.
[10] Thielen P, Fine M. Fatigue crack propagation in 4140 steel. Metall Trans A 1975;6:2133–41.
[11] Davis , editor. Metals handbook: desk edition. 2nd ed., ASM International; 1998.
[12] Honeycombe RWK, Bhadeshia HKDH. Steels: microstructure and properties. 2nd ed. Oxford, UK: Butterworth Heinemann; 2000.
[13] Bhadeshia HDK. Bainite in steels: transformations, microstructure and properties. 2nd ed. London: The University Press; 2001.
[14] ASTM Standard E8/E8M – 15a – Standard test methods for tension testing of metallic materials. West Conshohocken, n.d.
[15] Lee W-S, Su T-T. Mechanical properties and microstructural features of AISI 4340 high-strength alloy steel under quenched and tempered conditions. J Mater Process Technol 1999;87:198–206.
[16] Leen SB, Hyde TH, McColl IR, Williams EJ, Ratsimba CHH, Williams EJ, et al. An investigation of the fatigue and fretting performance of a representative aero-engine spline coupling. J Strain Anal Eng Des 2002;37:565–83.
[17] Hong J, Talbot D, Kahraman A. Load distribution analysis of clearance-fit spline joints using finite elements. Mech Mach Theory 2014;74:42–57.
[18] Ding Y, Jones R, Kuhnell BT. Elastic-plastic finite element analysis of spall formation in gears. Wear 1996;197:197–205.